
Proceedings Paper:
El-Jummah, AM, Andrews, GE and Staggs, JEJ (2013) Conjugate Heat Transfer CFD Predictions of Impingement Jet Array Flat Wall Cooling Aerodynamics with Single Sided Flow Exit. In: 2013 Proceedings of the ASME Turbo Expo 2013: Turbine Technical Conference and Exposition (GT2013). ASME Turbo Expo: Turbine Technical Conference and Exposition, 03-07 Jun 2013, San Antonio, TX, USA. American Society of Mechanical Engineers . ISBN 978-0-7918-5517-1

https://doi.org/10.1115/GT2013-95343

Proceedings of ASME Turbo Expo 2013: Power for Land, Sea and Air GT2013
June 3-7, 2013, San Antonio, Texas, USA

GT2013-95343

Conjugate Heat Transfer CFD Predictions of Impingement Jet Array Flat Wall Cooling Aerodynamics with Single Sided Flow Exit.

Abubakar M. El-Jummah, Gordon E. Andrews and John E.J. Staggs

Energy Research Institute
School of Process, Environmental and Material Engineering
University of Leeds
Leeds LS2 9JT, UK

ABSTRACT

Conjugate heat transfer CFD studies were undertaken on impingement square jet arrays with self induced crossflow in the impingement gap with a single sided exit. The aim was to understand the aerodynamic interactions that result in the deterioration of heat transfer with axial distance, whereas the addition of duct flow heat transfer would be expected to lead to an increase in heat transfer with axial distance. A square array of impingement holes was investigated for a common geometry investigated experimentally, pitch to diameter ratio X/D of 5 and impingement gap to diameter ratio Z/D of 3.3 for 11 rows of holes in the crossflow direction. A metal duct wall was used as the impingement surface with an applied heat flux of 100kW/m^2, which for a gas turbine combustor cooling application operating at steady state with a temperature difference of ~450K corresponds to a convective heat transfer coefficient of ~200W/m^{2}K. A key feature of the predicted aerodynamics was recirculation in the plane of the impingement jets normal to the cross-flow, which produced heating of the impingement jet wall. This reverse flow jet was deflected by the cross flow which had its peak velocity in the plane between the high velocity impingement jets. The cross-flow interaction with the impingement jets reduced the interaction between the jets on the surface, with lower surface turbulence as a result and this reduced the surface convective heat transfer. A significant feature of the predictions was the interaction of the cross-flow aerodynamics with the impingement jet wall and associated heat transfer to that wall. The results showed that the deterioration in heat transfer with axial distance was well predicted, together with predictions of the impingement wall surface temperature gradients and the pressure loss.

NOMENCLATURE

A Impingement hole porosity = $\pi D / (4X^2)$
C_d Impingement hole discharge coefficient Eq. 5.
D Impingement hole diameter, m
G Mass flow rate per hole / X^2 bar kg/sm^{2}bar
G_1 Mass flow rate at the first hole, kg/sm^{2}bar
G_N Mass flow rate at the N^{th} hole, kg/sm^{2}bar
h Impingement jet surface heat transfer coefficient, W/m^{2}K
L Target wall metal thickness, m
I Turbulence intensity assumed in V_{in} in the CFD
n Number of rows of holes upstream of a position in the crossflow.
N Number of rows of impingement holes in the crossflow direction.
Nu Nusselt Number
Nu_o Nusselt Number at the first impingement jet.
P Static pressure upstream of the impingement wall, Pa
ΔP Impingement wall pressure loss, Pa
R Gas constant for air, 287 J/kgK
Re Impingement hole Reynolds number
T_∞ Coolant temperature, 298K
U_j Impingement jet mean velocity, m/s
U_c Impingement gap cross flow velocity at hole N, m/s
V_{in} Uniform hole approach velocity over area X^2
X Impingement hole square array pitch, m.
y See Eq. 3
Z Impingement gap, m.

INTRODUCTION

The future advances in power generating gas turbine (GT) thermal efficiency rely on improved wall cooling of the GT components. This is because GT combustion temperatures that influence the efficiency are well in excess of the melting point of the metal material of combustor walls and turbine blades [1, 2]. The combined use of effective cooling techniques with sufficient thermal resistance material walls is the reason that high temperature operation of the GT components can be achieved. Impingement air jet cooling has been shown to be one of the most effective cooling technologies [3-8]. It enables the cooling air used to be minimized, which for turbine blades improves the cycle thermal efficiency and lowers carbon dioxide (CO_2) emissions.

The impingement geometry investigated here is typical of low NOx primary zone combustion chamber wall where the impingement efflux is discharged as the main combustion air, as shown in Fig. 1 [9]. Impingement cooling is also used for cooling combustor transition ducts or for the primary low the NOx region only and then the impingement air is passed into

combustor as film cooling or as part of the dilution air. This method of primary zone cooling is used in several industrial gas turbines. The geometry, shown in Fig. 2, in terms of X/D and Z/D, is also similar to those used in turbine blade cooling and was investigated experimentally by Florschuetz et al. [10]. Horlock et al. [11] have shown that film cooling of turbine blades results in the deterioration of the turbine efficiency. The maximisation of impingement cooling enables the film cooling mass flow to be minimised and hence has an impact on cycle efficiency.

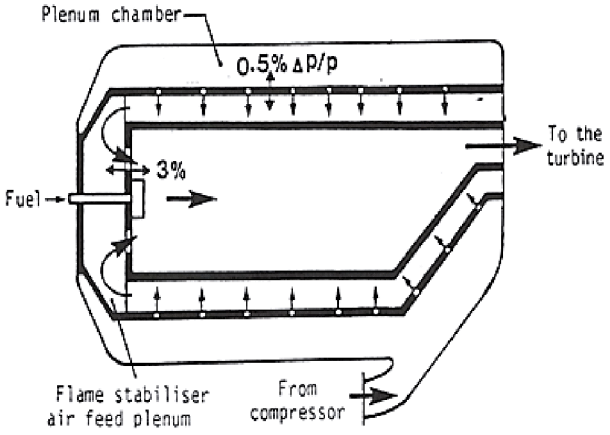

Fig.1: Schematic of regenerative cooled combustor with no dilution air flow [9].

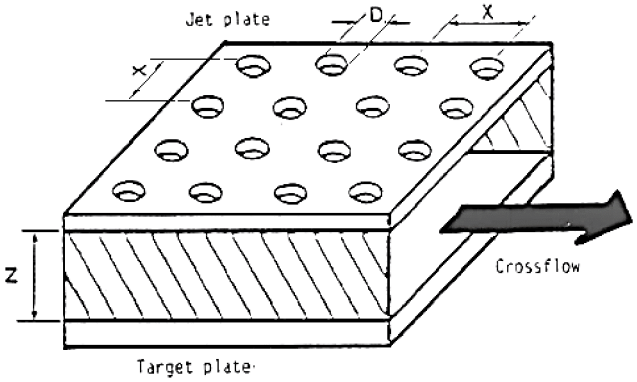

Fig.2: Multijet Impingement cooling Geometry showing maximum cross-flow scheme [9]

Chance [7] showed that a significant problem with impingement cooling was that the outflow of air in one direction led to a deterioration in the wall heat transfer. This is a problem in cooling design, particularly for combustor walls where the distances to be cooled are greater than in turbine blades. However, the reasons for this deterioration in heat transfer are not well understood and are often simply ascribed to the deflection of the impingement jet by the cross flow. However, the experimental results [7] showed that for high X/D with very high air jet velocities and relatively low impingement gap crossflow velocities, this deterioration of heat transfer with axial distance still occurred. As the flow in a duct has a significant heat transfer on its own [12] if the impingement and duct flow heat transfer were additive then the heat transfer would increase in the downstream direction and this does not occur in any experiments on impingement heat transfer with single sided exit.

The purpose of this work was to use CFD to understand the complex flows in the impingement duct and the interactions with the outflow from the upstream impingement holes by the downstream impingement jets. Andrews *et al.* [8] carried out a previous CFD investigation into the present geometry, but used a rather coarse grid. Their results considerably underestimated the observed convective heat transfer [9]. However, this work did highlight two important observations: the aerodynamic flow in the duct is complex and poorly understood and a higher grid resolution is required.

In practical applications of combustor wall cooling, the lengths that must be cooled necessitate a large number of holes. Obviously increasing the number of holes adds to the computational overhead in CFD. There have recently been several CFD investigations of the aerodynamics of impingement cooling [13-15] but none apart from Andrews et al. [8] has investigated more than 5 rows of holes and most have minimised the cross flow with exits from the gap on all sides. Andrews and co-workers have experimentally investigated up to 25 rows of holes [5, 9, 16-20]. In this work an 11 row impingement cooling system at an X/D of 5 and Z/D of 3.3 was modelled.

REVIEW OF CROSS-FLOW EFFECTS

Experiments on the influence of cross-flow on impingement heat transfer have used both a single row [21] and multi-jet arrays [6, 19, 21-23]. Most investigators found that cross-flow reduced the impingement heat transfer [7], even though the impingement jet velocity was high and the jet deflection by the cross-flow was small [9, 16, 17, 24]. Florschuetz *et al.* [10] found for a 10 row impingement array that the trailing edge heat transfer was between 20 and 41% below that of the leading edge for a range of geometries, most of which had flow maldistribution. Kercher and Tabakoff [6] found the trailing edge heat transfer lower than the leading edge heat transfer by between 5 and 41% depending on the geometry. The greatest effect was for N=12, X/D=6.3 and Z/D=3.9, which is similar to the geometry investigated in the present work.

Dyban *et al.* [22] varied N from 6 to 20 for 8 geometries without flow maldistribution. The results showed a reduction of heat transfer from the leading to the trailing edge of between 14 and 59%. The greatest effect was for N=20 with an X/D of 6. Obot and Trabolt [26] investigated the impingement cooling geometry N=12, X/D=5.6 and Eq. 1 predicts a 37% reduction in the heat transfer from the leading to trailing edge. For a Z/D of 6 the measured reduction was 34% in good agreement with Eq.1.

Bailey and Bunker [27, 28] presented results for impingement heat transfer with self induced cross-flow. They used square array jets, as in the present work, with X/D of 3, 6 and 9, but only the results for X/D of 3 and 9 were presented in detail in the paper. The X/D of 3 configuration was dominated by flow maldistribution influences, as expected. However, in most of this work for a fixed impingement plate length, X/D

was varied at constant D so that the number of rows of holes was decreased as X/D was increased. Any influences of cross-flow on the axial variation of heat transfer are strongly dependent on the number of upstream rows. Only in one geometry was the X/D of 9 tested with a hole size half that of the standard hole size and hence with twice the number of upstream rows of impingement jets.

In most of the work of Bailey and Bunker [27, 28] with X/D of 6 and 9, there were only four rows of holes. This is insufficient for the aerodynamics investigated in the present work to develop. Bailey and Bunker found very little influence of axial distance on the heat transfer for an X/D of 9 with four rows of holes, but there was a more significant influence for 9 rows of holes. For the highest hole Re tested with 9 rows of holes the trailing edge had 14% lower heat transfer than the leading edge, which was in reasonable agreement with Florschuetz *et al.* [10], who had a 15% decrease in heat transfer at the trailing edge for a similar geometry. For the Bailey and Bunker geometry with an X/D of 9 and Z/D of 5.5 Eq. 1 predicts a 17% decrease in heat transfer and hence is a reasonable predictor of their results.

The correlation of impingement heat transfer in the work of Bailey and Bunker [27, 28] did not specifically correlate the deterioration in heat transfer with axial distance, in a form similar to Eq. 1. The effect of the number of upstream rows of holes was not directly included in the correlation. However, the cross-flow to jet mass velocity ratio was included in the correlation and this decreases as the number of holes is increased, thus the number of upstream holes was indirectly taken into account.

Andrews and Hussain [16, 17] showed that the impingement heat transfer results of Chance [7], with no initial cross-flow, could be correlated by Eq.1.

$$Nu/Nu_o = 1 - 0.188\ (ND/X) \qquad (1)$$

This equation was shown to be applicable to the data of a wide range of investigators, including the well known results of Kercher and Tabakoff [6]. It should be noted that the impingement gap size, Z, is not a factor in the deterioration of the heat transfer with distance. This was because the impingement jet velocity at the surface decreased with increasing Z (as did the cross-flow velocity), thereby ensuring that there was little change in the surface jet to cross-flow velocity, even though the mean jet to cross-flow velocity increased as Z increased. Equation 1 is mainly based on the results of Chance [7] who showed that it was valid for 2 <Z/D <8 and for X/D values with no flow maldistribution. The lack of dependence of Eq. 1 on Z does not mean that there is no effect of Z or Z/D on the heat transfer as there will be the usual dependence of Nu_o on Z/D [5, 16].

Abdul Hussain and Andrews [9] investigated impingement heat transfer with a single sided exit and no initial cross-flow, for the 10 row impingement geometries similar to those that are modelled in the present work. Fig. 3 shows the decrease in heat transfer coefficient (HTC) with axial distance for an X/D of 4.7 and three coolant mass fluxes, G kg/sm^2. This shows good agreement with the results of Chance [7] and also approximately supports Eq. 1. However, there was a deviation with slightly higher values at the trailing edge. This is due to the problem of flow maldistribution that occurs due to the cross-flow pressure loss being significant relative to the impingement wall pressure loss.

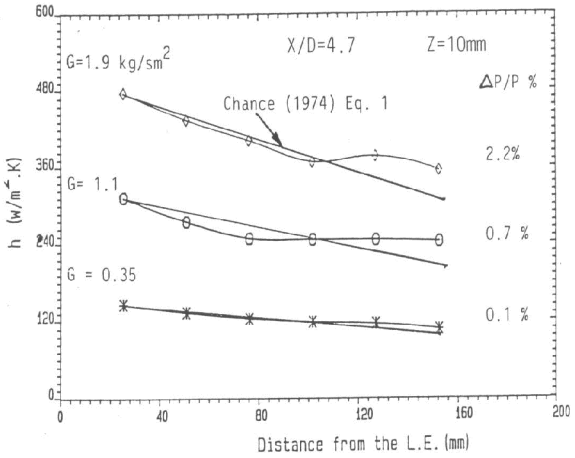

Fig.3: Impingement HTC as a function of axial distance for X/D of 4.7 for three flow rates.

Fig. 4 outlines the pressure loss differences that result in air being moved from the leading edge to the trailing edge. A prediction of the geometrical conditions under which flow maldistribution would occur was made by Andrews and Hussain [16, 17]. They showed that the ratio of the impingement jet velocity, Uj, to cross-flow mean velocity, Uc, was given by Eq. 2, for 2<Z/D<8.

$$Uj/Uc = Z/(NAX) = 4/\pi\ (ZX) / (D^2 N) \qquad (2)$$

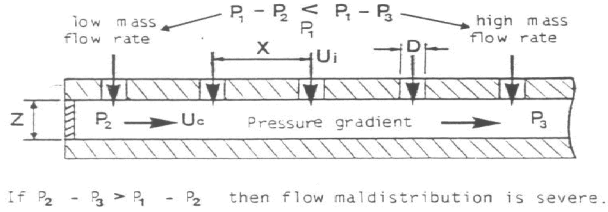

Fig.4: Impingement with cross-flow illustrating the generation of cross-flow pressure gradients.

An expression basically similar to Eq.2 was presented by Gaunter (25). Andrews and Hussain (17) reviewed the available data on impingement heat transfer and showed that if Uj/Uc was less than 2 then flow maldistribution was significant.

Andrews and Hussain [16, 17] showed that the flow maldistribution, G_N/G_1, could be predicted for incompressible jet flow from the ratio y of jet to cross-flow pressure loss, Eq. 3, as in Eq. 4.

$$y = \left(\frac{Z}{C_d nAX} \right)^2 \qquad (3)$$

$$\frac{G_N}{G_1} = \frac{y}{1-y} \tag{4}$$

$$G = C_d A [(2/RT)(\Delta P/P)]^{0.5} \tag{5}$$

Where, C_d is the discharge coefficient of the impingement hole defined by Eq. 5.

Equation 3 shows that if y is large then the flow maldistribution will be large. Decreasing Z or increasing N, A or X will make the flow maldistribution increase. The X/D effect is illustrated in Fig. 5, which shows for a constant G and constant Z of 10mm (constant Uc) the axial variation of h for various X/D. This shows that an X/D of 4.7 is near the limit of X/D for flow maldistribution to be small. The present CFD predictions were carried out to compute the flow maldistribution for an X/D = 5, taking into account the influence of the cross-flow, which is ignored in the above 1D analysis. However, the results do show a small but significant effect of the cross-flow on maldistribution at X/D = 5. In this case the ratio of Uj/Uc at the last row of holes was 2.1. For X/D < 3.8 the flow maldistribution leads to an increase in h in the trailing edge region, whereas with no flow maldistribution Eq. 1 applies and h decreases with axial distance. Flow maldistribution increases as Z is decreased and this decreases Uj/Uc, thus a small Z/D and small Uj/Uc result in flow maldistribution in many cases.

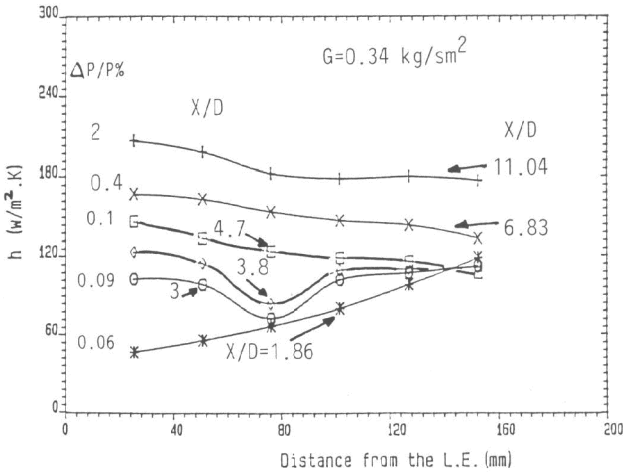

Fig.5: Impingement heat transfer with cross-flow, the influence of X/D at constant coolant mass flow rate at constant Z=10mm and X=15.2 mm.

The deterioration of impingement heat transfer with distance from the first row of holes for large X/D (>~4) is unexpected. As the addition of cross-flow or duct flow heat transfer to the impingement heat transfer would be expected to result in an increase in the heat transfer with distance from the first jet due to the additional heat transfer created by the cross-flow [12]. However, Andrews and Hussain [16, 17] showed that, for an impingement X/D of 7, the duct flow heat transfer was only significant relative to the impingement heat transfer for Z/D<1. Hence, in many practical geometries duct flow heat transfer may not be a significant part of the overall heat transfer.

REVIEW OF CFD INVESTIGATIONS

Previous CFD investigations of impingement cooling have not been primarily directed at the cross flow effect and have not used a large number of upstream holes, apart from a previous attempt at this configuration by Andrews *et al.* [12] with a much coarser grid than in the present work. The complex recirculation in the impingement gap and the interaction between adjacent jets on the target surface presents a challenge for CFD predictions.

The flow distribution and the heat transfer coefficients *h*, on the liner of gas turbine combustor for jets impingement and cross-flow were predicted by Bailey *et al.* [28]. Both structured [13, 28, 29] and unstructured [30] or hybrid [31] grids have been used depending on the complexity of the geometry. The use of steady state isothermal conditions that were employed experimentally [5, 19] was also applied for the CFD impingement analysis [8, 29]. Usually cooling air was at ambient temperatures ~300K, with a range of inlet velocities that determines the hole Reynolds number, Re [31]. Often, impingement cooling CFD investigators uses the RANS turbulent models, especially the two equation model [13, 28], because the turbulence is considered to be isotropic in the complex stirred flow in the impingement gap.

CFD simulation enables the prediction of the flow fields that characterizes air jet impingement cooling [32]. The work of Taslim and Rosso [13] shows particle tracer air flow patterns within the impingement gap and this technique was also used in the present work. Heat transfer characteristics were also shown to be predicted with the use of conjugate heat transfer [33]. The present CFD work uses conjugate heat transfer and also visualizes the heated coolant flow reflected from the hot target surface using dimensionless temperature contours.

CFD METHODOLOGY

Model Geometry and Boundary Conditions

The impingement heat transfer system used for this investigation is shown in Fig.2 and is similar to that used by other investigators [7, 9, 26]. This is also similar to the experimental test facility used by Andrews and Hussain [5]. It consists of an internal cross-sectional area of 152mm square test section with a plenum chamber that was lagged with 25mm thick thermal insulation, which is considered as a boundary condition with no heat flux in the computation. Compressed air at an ambient temperature of ~300K flows through the plenum inlet from the supply [20]. This coolant air then flows through the array of holes to cool the metal target wall below. The hot gas flow in the duct below the target wall was not modelled explicitly. Instead a constant heat flux of 100kW/m^2 was applied as the boundary condition along the target wall at an impingement gap, Z, of 10mm. This heat flux approximately reproduces the conditions of the hot rig of Abdul-Hussain *et al.* [9], with a coolant to hot gas temperature difference of ~450°C and convective heat transfer coefficient at the cooled surface of ~200W/m^{2}K.

In this work two metal surfaces were investigated: aluminium, representing the extreme condition of very good internal wall heat transfer and nimonic 75 which was the combustor liner wall material used in the experimental work.

There was a factor of 20 difference in the two thermal conductivities. A highly conductive wall is a common feature of experimental work with hot impingement targets, as copper walls are often used [6, 7, 10]. The aerodynamics were not influenced by the wall thermal conductivity, but the heat transfer coefficient and the wall temperature distribution was affected, with the aluminium wall being predicted to be at a uniform temperature across all 11 impingement jet regions.

Computational grid

The impingement geometry shown in Fig.6 was modelled using the symmetrical schematic representation shown in Fig.7. The impingement geometry was a square array of holes with an X/D of 5.0 and 11 rows of air holes. An additional row of holes was added to the model compared with the experiments to avoid any passage end effects in the modelling. The specific geometry modelled in the present work is given in Table 1. It has an impingement air hole wall thickness of 6.35mm and is typical of that used in some large industrial gas turbine combustors.

The three dimensional model was discretized using a structured grid with the ANSYS ICEM meshing tool. The cell concentration was higher at the impingement and target wall surfaces. These surface walls are represented by cells of the same cross sectional area that are rectangular but quadrilateral around the air hole surfaces as shown in Fig.7 and Fig.8.

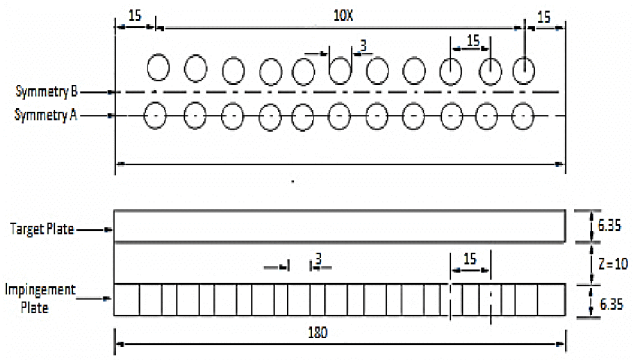

Fig.6: Symmetrical element of the computational domain for one row of air holes using single exit flow.

Table 1: Geometrical Parameters

Description	Values
D	3.0mm
X	15.0mm
Z	10.0mm
L	6.35mm
X/D	5.0
Z/D	3.3
N	4444m^{-2}
Array	10 × 11
A	3.14%
y	7.04

Turbulence Model

The standard k-ε turbulence model was used for the calculations presented below. The effects of other turbulence models was investigated, but are not reported here. The differences were not substantial and all the flow features had similar predictions.

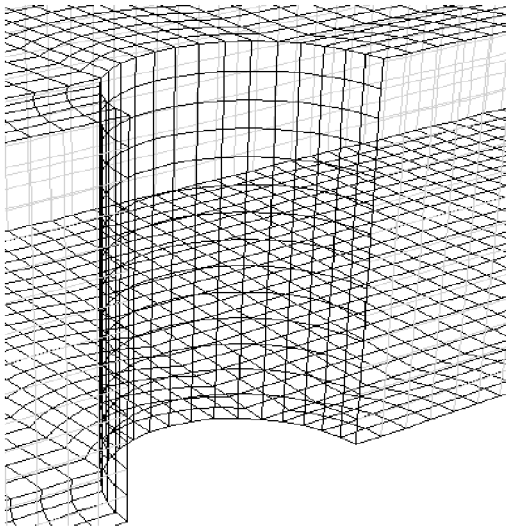

Fig.7: Impingement plate air hole grid

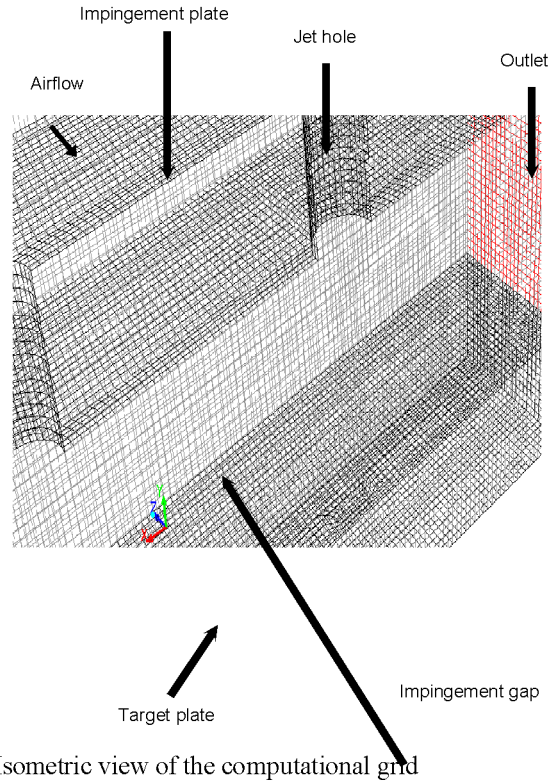

Fig.8: Isometric view of the computational grid

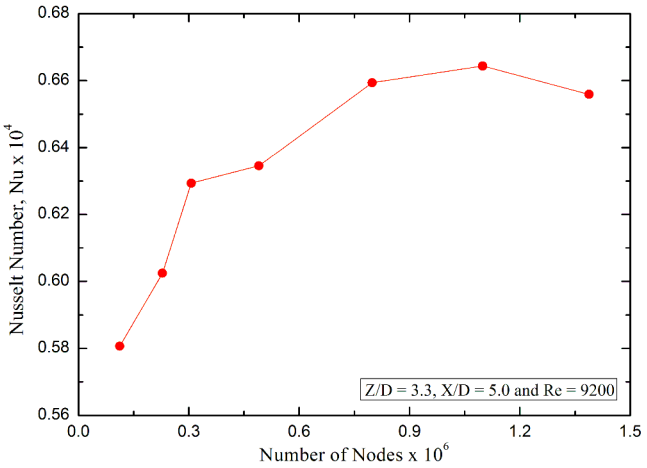

Fig.9: Grid Independence test for range of grid cells.

Table 2: Air Flow Conditions

Description	Values
G	1.9kg/sm^{2}bar
V_{in}	1.6m/s
T_∞	298K
ρ	1.178kg/m^3
q''	100kW/m^2
I	5.1%
Re	9200

Grid sensitivity

A grid independence test for a range of grid cells from 10^5 to ~1.5×10^6 was carried out. A representative Nusselt number at the target wall was computed to investigate the influence of the number of computational cells on heat transfer. The results are shown in Fig.9 and indicate that at least 10^6 cells are required to reduce grid sensitivity effects. The impingement flow conditions that were used are shown in Table 2. It was found that the range of values tested that produced insignificantchange in the results was for cells between 0.8 to 1.45 million. Therefore, the grid cells of 1.3×10^6 with ~1120 nodes (~60 nodes/plane) in each air hole (Fig.8), was chosen for the CFD investigations. This was considered to be sufficient to resolve any influence of the cross-flow on the velocity profile of the impingement jet discharge, as well as to compute the flow separation at the air hole inlet.

VELOCITY, TURBULENCE AND IMPINGEMENT HOLE FLOW MALDISTRIBUTION IN THE IMPINGEMENT GAP

Velocity profiles

The predicted flow pattern is represented in contour plots and x-y plots for the velocity, static pressure, shear stress and turbulent kinetic energy (TKE). The variation of static pressure loss along the impingement gap is presented as this is determined by the flow aerodynamics and was also measured in the experimental work. Also presented are the spatial distribution of the heat transfer coefficient and the wall temperature distribution.

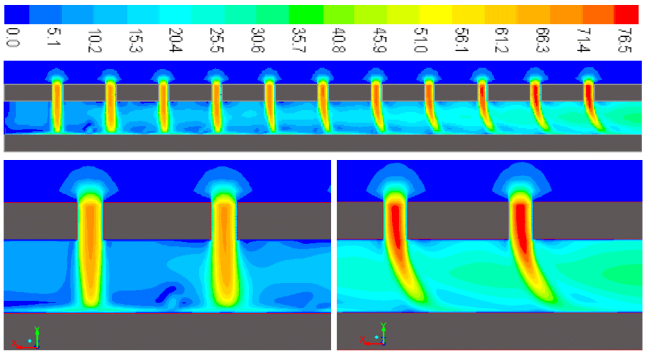

Fig.10: Impingement gap contour of velocity magnitude (m/s). Complete gap flow at the top and the first (left) and last (right) two holes at the bottom.

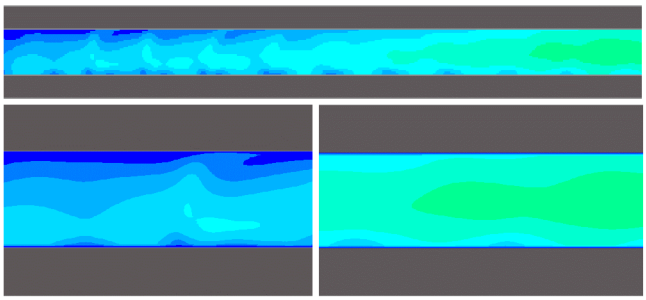

Fig. 11: Velocity magnitude (m/s) on the centreline between the jets in Fig.10 with same scale

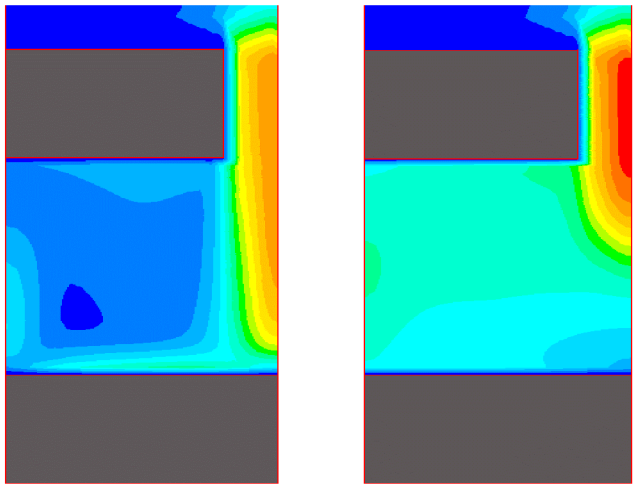

Fig. 12 Velocity profiles at 90° to the cross-flow on the centreline of the impingement jet. Second hole on left and last hole on the right. Same scale as Fig.10.

Figure 10 shows the magnitude of the air jet velocity in each hole and in the impingement gap for the plane on the centreline of the impingement jets. Figure 11 shows the velocities in the plane between the impingement jets in Fig.10. It is in this plane that the cross-flow velocity is at a maximum, so the velocities are low at the leading two holes and increase at the last two holes. The highest velocity is in the centre of the

duct. Figure 11 shows that a reverse jet in the leading hole area was predicted, that flows in the opposite direction to the impingement jets and on the centre point between a four hole array of impingement jets. After the fourth row of holes the cross-flow has blown this reverse flow jet away.

Figure 12 shows the velocity profiles in the plane at 90° to those in Figs.10-11 on the centreline of the holes. This is shown for the second and last hole. The cross-flow passes between the jets and this is a low velocity at the second hole as there is only one upstream hole, but it increases significantly at the last hole. At the last hole the coolant jet is deflected away from being inline with the hole and hits the target surface further downstream, as shown in Fig.10.

The 3D particle paths of Fig.13 show the reverse jet flowing between the impingement jets between the first two rows of holes. The reverse flow jet is already deflecting towards the exit plane and this trend increases along the gap to the exit plane. Fig.13 shows that this centreline reverse flow jet is deflected by 45° and is intensified by the cross flow.

This jet has a strong impingement on the impingement air hole wall, well downstream of the jets that started the interaction as shown in Fig.10. However, this impingement is at a lower velocity then at the leading edge and the distribution of turbulence around the jet is advected downstream, as will be shown below.

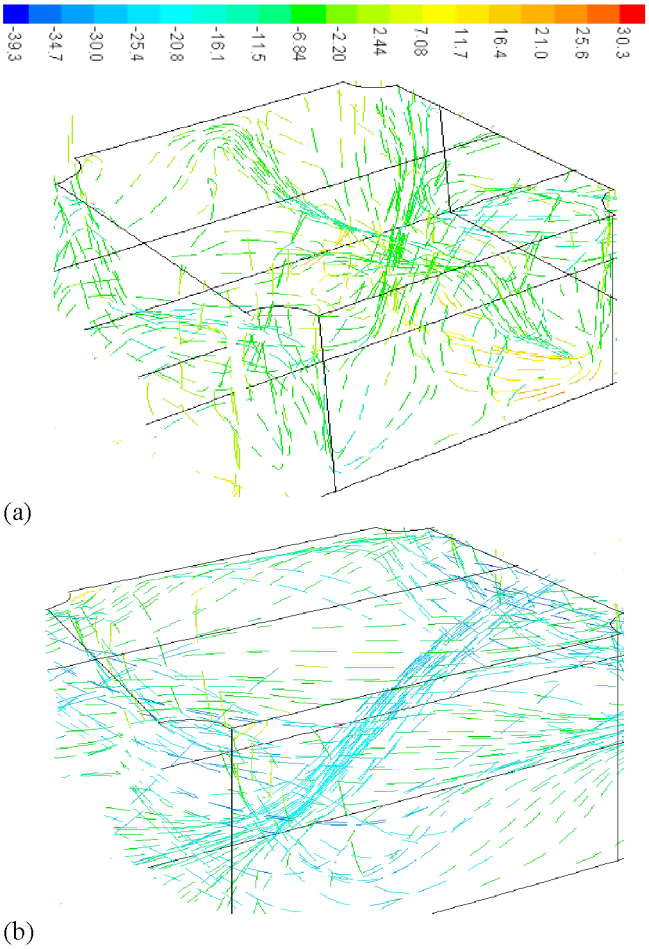

Fig.13: Impingement gap pathlines of x-velocity vector (m/s) (a) upstream air jet flow (b) downstream air jet flow

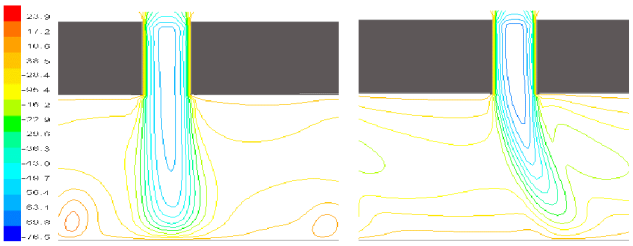

Fig.14: Impingement hole contour of y-velocity vector (m/s)

Flow Maldistribution

The velocity contours on the centre line of the first and last jet are shown in Fig.14. This shows that the flow at the jet outlets is not uniform with axial distance. This is verified by the outlet jet velocity profiles in Fig.15. None of the profiles are fully developed turbulent flow and at the leading hole the profile is symmetric and closer to parabolic than the flatter turbulent pipe flow velocity profiles. This is because of the sharp edged entry to the impingement hole from the plenum chamber and the flow separation at the hole inlet. This is followed by flow attachment to the impingement hole wall about half way long the short holes. There is then insufficient distance to achieve fully developed pipe flow turbulence. At the last hole the presence of the cross-flow acts to skew the velocity profile at the hole outlet in the downstream direction. This will be shown below to result in a distortion of the impingement heat transfer and turbulence in the downstream direction on the target plate.

The predicted impingement hole velocity enables the mean velocity of each hole to be determined. This velocity was calculated in the middle of the hole, to avoid any inlet and outlet flow recirculation zones. The mean velocity for each hole is shown in Fig.16, normalised to the mean velocity for all the holes, which is set by the total mass flow of coolant for which the computation is carried out, as detailed in Table 2. Fig.16 shows that the geometry investigated did have a flow maldistribution with the leading holes receiving 7% less air and the last holes receiving 9% more air. This is in excellent agreement with the simple 1D computation of Eq.4, which also predicts a total flow maldistribution of 16%. This strongly supports the view that the flow maldistribution is driven by the static pressure difference along the duct, as depicted in Fig. 4.

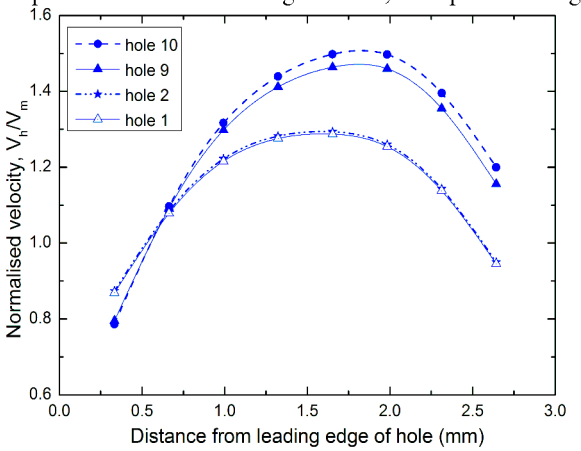

Fig.15: Impingement air hole velocity profile

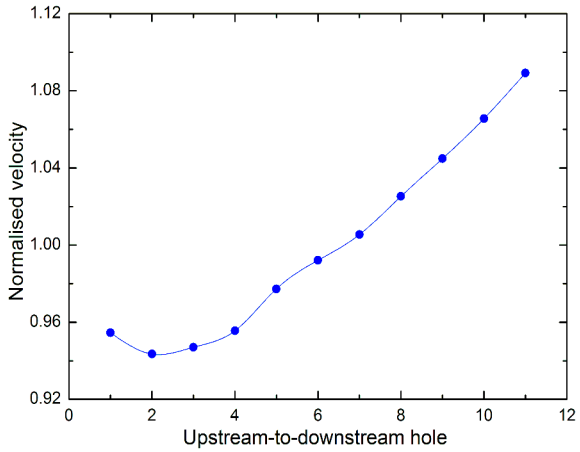

Fig.16: Coolant jet flow maldistribution of the impingement hole.

Static Pressure Loss along the Impingement Gap

The predicted static pressure loss across the impingement wall as a function of axial distance is shown in Fig.17. This was determined as the pressure difference between the air supply plenum chamber and the static pressure on the impingement gap side of the impingement wall at the centre of the four hole impingement hole. Fig.17 clearly shows that the lower flow through the leading holes gave a lower pressure loss. The difference in static pressure between the first hole pressure loss and the last is the pressure loss of the cross-flow down the gap and added 0.45% pressure loss to that across the first hole. This crossflow velocity pressure loss is the source of energy for the generation of turbulence by the cross-flow as it interacts with the impingement jets. The predicted overall pressure loss of 2.45% is in excellent agreement with the measured pressure loss of 2.4% at this flow condition. This indicates that the flow aerodynamics in the holes and the gap are correct, as these determine the pressure loss.

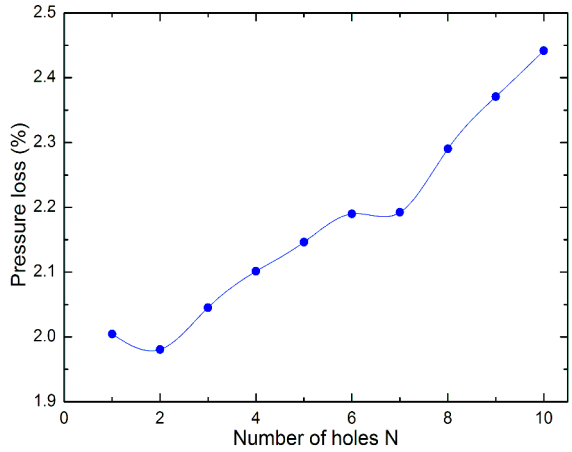

Fig.17: Impingement air flow pressure loss with distance

Target Wall Static Pressure Distribution

The predicted static pressure contours are another way of visualizing surface velocity effects. High local velocities have low static pressures and areas that generate turbulence have

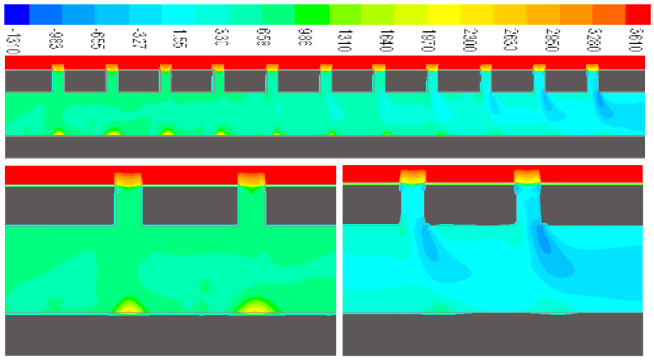

(a)

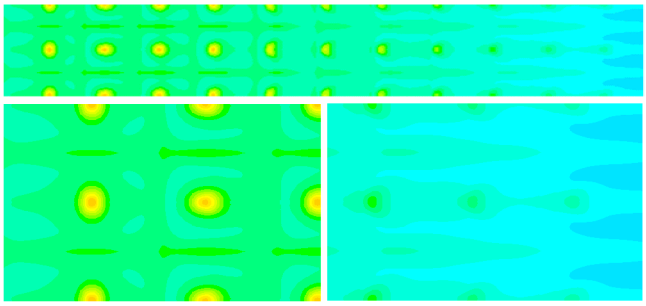

(b)

Fig.18: Static pressure distribution (Pa) (a) in the plane of the impingement jet for the full gap (top) and in detail for the first two holes (left) and the last two (right) (b) impingement target surface with the hole wall (top) and the leading two holes (left) and last two holes (right).

static pressure differences across the turbulence generation region. Fig. 18 shows the predicted static pressure distribution in the plane of the impingement jets (Fig. 18a) and on the impingement target surface (Fig.18b). The leading edge jets clearly impinge on the target surface and the flow stagnates and produces the highest static pressure. However, after the fifth jet this impingement region has gone and it is here that the heat transfer is predicted to deteriorate.

The higher velocity in the downstream jets due to flow maldistribution is also clearly seen in the lower static pressure. The strong static pressure gradients at the last two holes shows significant distortion of the flow profile due to the cross-flow. On the target surface the high static pressure between the jets and the low static pressure region after the impingement point followed by high static pressure at the impingement point of adjacent jets gives a good visualization of the complex flow pattern on the target surface. At the trailing edge most of this complex flow has been washed away by the cross-flow, leading to the observed reduced heat transfer.

Turbulent Kinetic Energy Distribution

The predicted spatial distribution of the turbulent kinetic energy is shown in Fig.19. The contours in the plane of the impingement jets in Fig.19a show high turbulence inside the impingement holes and peak turbulence in the shear layer at the edge of the impingement jets. In the downstream portion of the impingement gap the turbulence is deflected downstream and

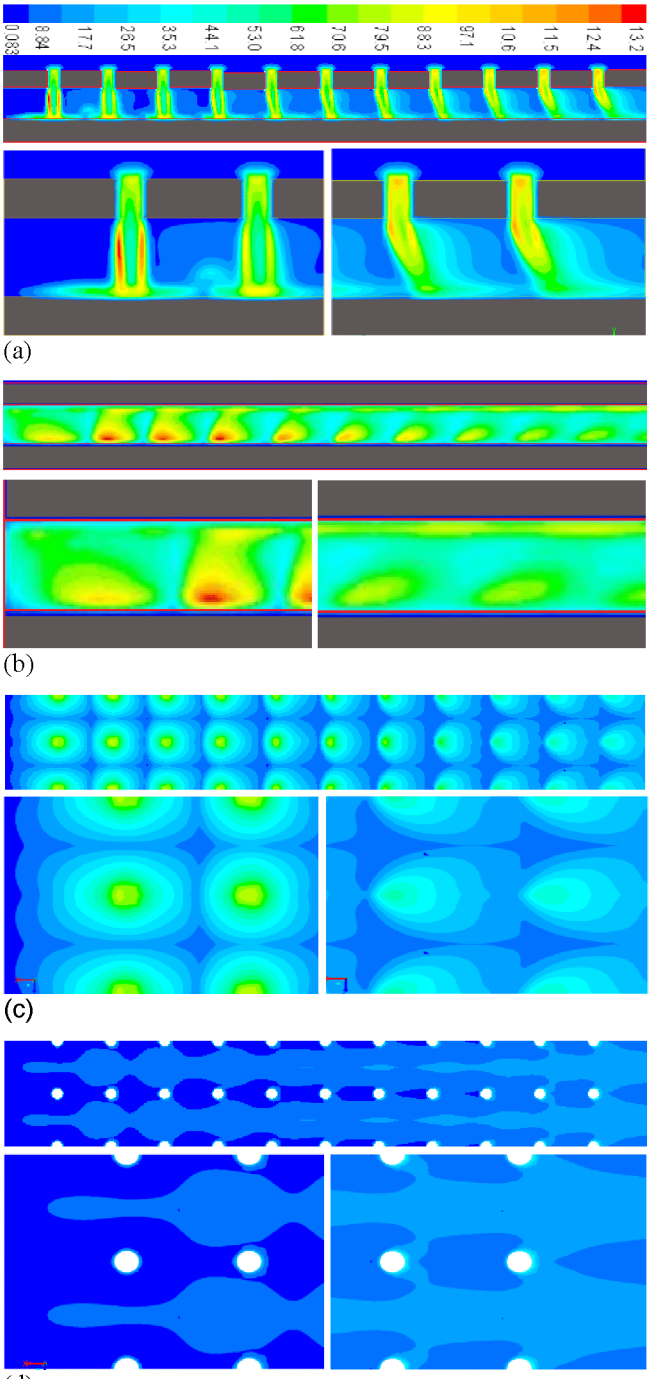

Fig.19: Contours of TKE (m^2/s^2) in the plane of the impingement jets (a), in the mid plane between the impingement jets (b), on the surface of the target plate (c) and on the impingement jet wall (d).

peak turbulence does not occur on the target wall. This leads to the reduction in heat transfer as shown later. The impingement jets flow along the surface with high turbulence and then impinge against each other. This gives another generation of turbulence between the impingement jets as shown in Fig. 19b.

Fig. 19c shows the distribution of turbulence on the impingement jet target surface. This shows that there is a peak turbulence zone on the surface in line with the jet impingement point, but this decreases with downstream distance. By the end two holes the peak turbulence layer is not in contact with the wall and has been lifted off the wall by the cross flow. This is the cause of the deterioration in the heat transfer in this region. On the target surface there are strong gradients of turbulence, but the surface area covered by high turbulence decreases with distance towards the gap exit.

On the impingement jet surface the opposite trend was predicted with low turbulence in the region of the leading two impingement holes with high surface spread of turbulence in the downstream last two jets. However, the turbulence on this surface is much lower than that on the target surface at all axial locations. However, it can be seen that the peak turbulence is between the impingement jets where the reverse flow hits the impingement wall surface.

Shear Stress Surface Distribution

Regions of high shear stress generate turbulence. The shear stress distribution on the target surface is shown in Fig. 20. This shows for the first two holes the strong shear region at the edge of the impingement jet. The centre of the jet is low shear as that is still in the potential core region of the jet. The Z/D of the jets is 3.3 and this is shorter than the potential core of free jets, so the central region is the original impingement jet central flow region with little shear. Around this jet is the turbulent shear layer, as shown in Fig.20.

The action of the cross-flow was predicted to distort this region and by the last two holes the shear stress region has the suggestive shape of a horseshoe vortex on the surface. This is very similar to the interaction of cross-flow with film cooling jets, where horseshoe vortices also occur due to the interaction of the cross-flow and the film cooling flow. It is clear that the strong shear regions are no longer attached to the surface or cover sufficient area to give turbulence generation and again it is part of the reason why the heat transfer deteriorates in the downstream part of the impingement gap.

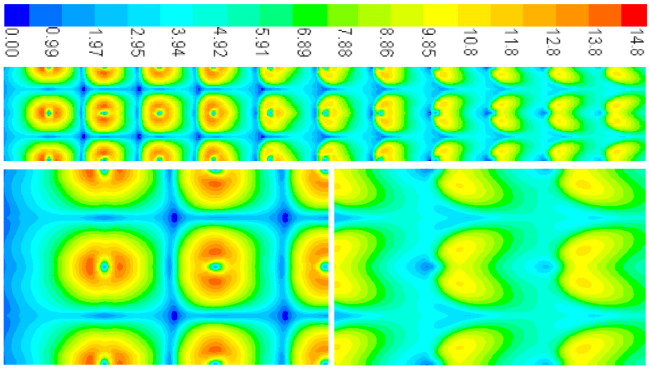

Fig.20: Shear stress (Pa) on the target plate surface

CONVECTIVE HEAT TRANSFER RESULTS

Nusselt number contour plots are shown in Fig.21 on the target surface and also on the impingement jet wall. The profiles are very similar to those for turbulent kinetic energy, which clearly controls the convective heat transfer. The peak heat transfer

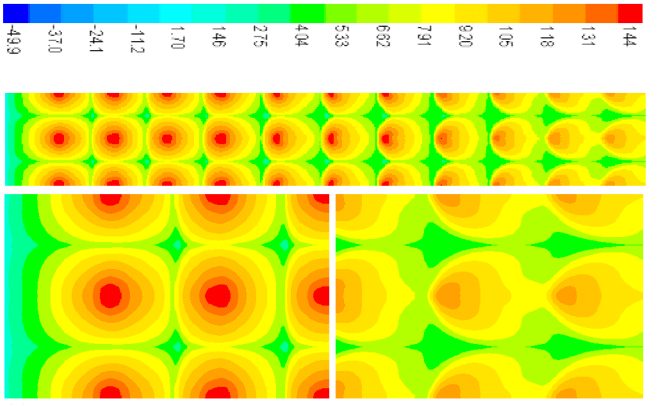

(a)

(b)

Fig.21: Contours of Nusselt number ($\times 10^2$) from the upstream to downstream for (a) Target plate (b) impingement plate

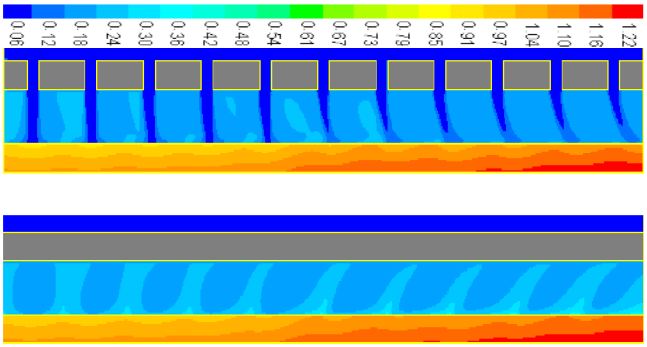

Fig.22: Contours of dimensionless air temperature in line with the impingement jets (top) and between the jets (bottom) for the Nimonic 75 wall cooling.

coefficient deteriorates in the downstream portion of the impingement wall, as found in the experimental work in Fig.3. There were regions of low heat transfer between the jets. On the impingement jet surface the heat transfer was much smaller but peaked in line with the reverse jets that flow in the centre of each four air hole impingement group. More heat transfer to this surface occurs with downstream distance.

An obvious feature of the heat transfer is that the longer the impingement air jets are in contact with the hot wall, the greater the temperature rise of the air jets will be. Thus the reflected jets are hotter than the impingement jets and the temperature of the cross-flow increases with axial distance. These trends were predicted and are shown in Fig.22 for the plane in line with the impingement jets and for the plane between the jets. The temperature contours are dimensional temperature ratios $(T-T_c)/(T_w-T_c)$.

Figure 22 clearly shows the direction of the cold jets penetrating though the hotter cross-flow air. In between the jets the central reverse flow jet is clearly seen as it is hotter than its surroundings. In the downstream area this reverse flow jet is deflected by the cross-flow. The hottest flow is clearly that of the cross-flow between the impingement jets.

The deterioration in heat transfer on the surface with distance was also shown by the generation of hot air adjacent to the surface near the last two holes. This was due to the reduced cooling heat transfer. This effect was greatest between the holes. Fig.22 also shows the temperature contours in the metal target wall, which shows the greater temperature gradients through the wall thickness compared with the axial gradients.

Axial Variation of the Surface Average Heat Transfer Coefficient, *h*.

The predicted heat transfer coefficient, h, was surface averaged for each impingement hole which cooled a surface area of X^2 of surface with in impingement jet directed at the centre. The axial variation of the averages is shown in Fig. 23. The numerical agreement in Fig.23 with the measured surface averaged values was very good at the leading edge for the nimonic 75 wall. However, for the aluminium wall the predicted h was too high and the wall was at a near uniform temperature throughout the length due to internal conduction. The nimonic 75 wall results agree perfectly for the first five impingment jets and then overpredict the measured locally averaged heat transfer coefficients on the experimental nimonic 75 wall [9]. The disagreement over the last five holes of the impingement gap is a maximum of 10% high at hole 7 for the CFD compared with the experiments. This indicates that the comlex flow in the trailing edge region,. With high impingement jet flow maldistribution and high crossflow interactions has not been adequately resolved by the CFD.

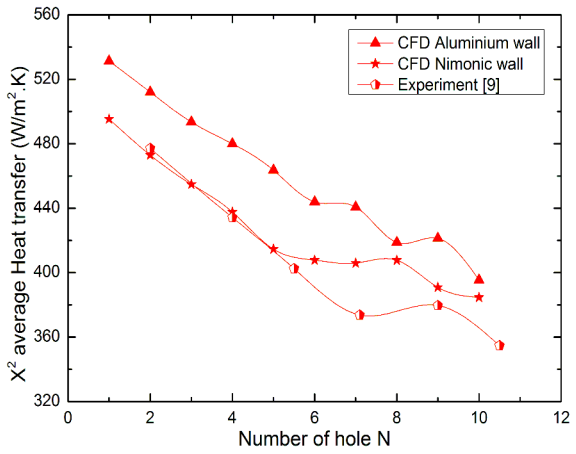

Fig.23: Surface average (over area X^2) heat transfer coefficient as a function of air hole number in the crossflow direction. Comparison with the experimental results of Abdul Husain and Andrews [9].

Figure 24 shows the predicted wall dimensionless temperature distribution for the nimonic wall. The dimensionless surface temperature parameter was $(T_w - T_\infty)/(T_m - T_\infty)$, where T_m was the mean wall temperature over all the holes in the crossflow direction. Figure 24 shows that the wall temperature varied between 22% above the mean and 15% below the mean. Wall temperatures were lower at the leading edge as expeted from the higher h in this region. At the leading edge the wall was cooler under the impingement jets and hotter between the jets, but this difference was only 6% of the mean temperature difference (about 20K). In the same region Fig.21 shows that the heat transfer coefficient varied by = - 37% of the mean, between the centre of the jet and the region between the jets. The thermal conduction in the wall ensures that the wall temperature smooths out these large gradients in heat transfer coefficient.

At the trailing edge of the impingement wall in Fig.24 shows that the wall is hotter than at the leading edge due to the lower heat transfer coefficients. The crossflow is now such an important part of the flow that the peak wall temperature is now between the impingment jets in line with the crossflow jets, which have been heated by the upstream jets. However, the temperature variations between the impingement jet and the midpoint is quite small at about 6% of the mean T_m-T_c as shown in Fig.24 at the trailing edge. The overall mean wall temperature gradient from the leading edge to the trailing edge was 16% of the mean wall temperature, which is about 53°C. This is much lower than the gradients in heat transfer coefficients shown in Fig. 21, due to the distribution of the heat within the wall by thermal conduction.

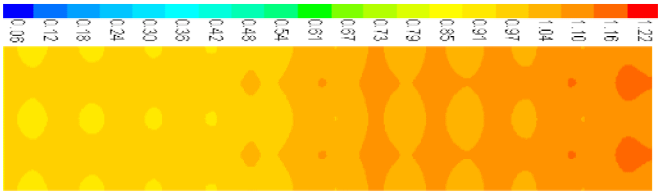

Fig.24: Predicted metal surface dimensionless temperature deviations from the mean wall temperature.

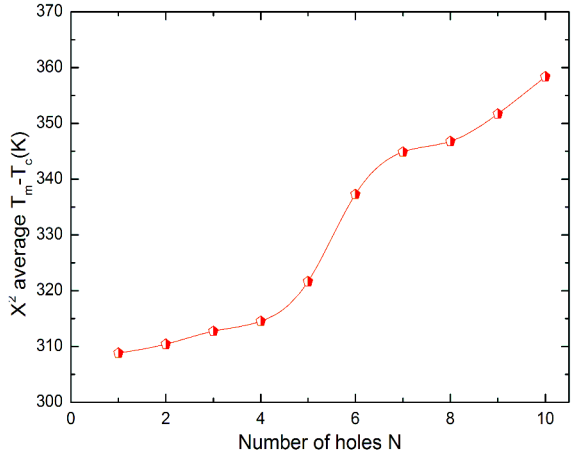

Fig.25: The predicted X^2 locally surfaced averaged temperature difference as a function of hole number in the crossflow direction.

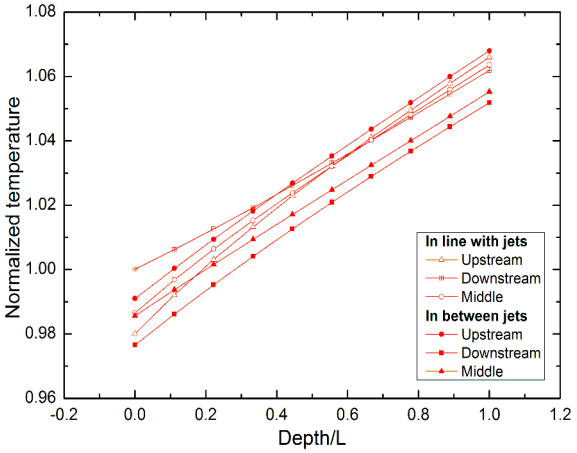

Fig.26: The temperature gradient through the wall thickness normalised to T_m in K.

The predicted temperature difference between the mean wall temperature, averaged over the surface area X^2 cooled by each impingement hole, and the coolant upstream temperature (T_m-T_c) is shown in Fig.25. This shows the hotter wall in the downstream edge of the wall , due to the deterioration in h with distance. The mean thermal gradient over the 10 rows of impingement jets is about 50K which is not of great concern from a thermal stress viewpoint. Fig.26 shows the thermal gradient through the thickness of the nimonic wall. The temperature was normalised to the mean surface averaged temperature T_m K for a range of positions on the impingement test wall. The depth/L of 1 is the surface directly exposed to the 100 kW/m^2 heat flux and is higher than the surface cooled by the impingement jets. This temperature gradient is significant at 40K over 6.35mm, which is 6.3K/mm compared with 0.33K/mm for the axial thermal gradient due to theo crossflow. Thus in terms of thermal stress it is the metal thickness where the thermal stress is most significant.

CONCLUSIONS

Conjugate heat transfer CFD studies were undertaken to try to elucidate the aerodynamic interactions that result in the deterioration of heat transfer with axial distance in impingement heat transfer with a single sided flow exit. A 10 row array of impingement holes was investigated for pitch to diameter ratio X/D of 5 and impingement gap to diameter ratio Z/D of 3.3 with square array holes, where flow maldistribution between the rows of impingement jets was small.

The CFD results show that the impact of the cross-flow was to strongly deflect the reverse flow jet on the centre of each of four hole impingement jets. The reverse jet was deflected at 45° by the 10th impingement hole position. The cross flow reduced turbulence levels on the impingement wall and this reduced the heat transfer coefficients.

The complexity of the aerodynamics of impingement flow with large numbers of holes and flow exit in one direction has been clearly demonstrated. The importance of the reverse impingement flow on the impingement jet surface has been

emphasised and the role of the cross flow in interacting with this reverse flow jet has been demonstrated.

The predicted axial variation of the heat transfer coefficent was well predicted, especially over the first 5 rows of holes. The agreement was not as good at the trailing edge. The predicted wall temperature profiles showed much lower temperature gradients than gradients in the surface heat transfer. This illustrates the action of internal wall conduction in smoothing out the large convective heat transfer gradients. The largest thermal gradients were predicted to be through the thickness of the wall at 6.3 k/mm

ACKNOWLEDGEMENTS

Abubakar M. El-jummah wishes to acknowledge the financial support from University of Maiduguri and the Government of Nigeria.

REFERENCES

[1] Brooks, F. J., "GE Gas Turbine Performance Characteristics," *GE Power Systems,* vol. GER-3567H, pp. 1-16, 2010.

[2] Eisako, I., Ikuo O., and Keizo T., "Development of Key Technologies for the Next Generation 1700°C-Class Gas Turbine," *Proc. ASME Turbo Expo 2009: power for Land, Sea and Air,* ASME Paper GT2009-59783, pp. 1-11, 2009.

[3] Kumada, M. and Mabuchi I., "Studies on the Heat Transfer of Impinging Jet," *1st Report, Mass Transfer for Two-Dimensional Jet of Air impinging Normally on a Flat Plate,* Vol. 13, No. 55, pp. 77-85, 1970.

[4] Facchini, B. and Surace M., "Impingement Cooling for Modern Combustors: Experimental Analysis of Heat Transfer and Effectiveness," *Experiments in Fluids. Springer,* vol. Vol.40, pp. pp.601-611, 2006.

[5] Andrews, G. E. and Hussain C. I., "Impingement Cooling of Gas Turbine Components," *High Temperature Technology,* vol. Vol. 2 No.2, pp. 99-106, 1984.

[6] Kercher, D. M. and Tabakoff W., "Heat Transfer by a Square Array of Round Air Jets Impinging Perpendicular to a Flat Surface including Effects of Spent Air," *ASME J. Eng. Power,* pp. 73-82, 1970.

[7] Chance, J. L., "Experimental Investigation of Air Impingement Heat Transfer under an Array of Round Jets," *Tappi,* vol. Vol.57, No.6, pp. 108-112, 1974.

[8] Andrews, G.E., Wang, J. and Abdul Hussain, R.A.A "CFD Predictions of the Aerodynamics and Heat Transfer from Arrays of Impinging Jets with Cross-flow". International Gas Turbine Congress 2011, Osaka, IGTC 2011-0141, 2011.

[9] Abdul Husain, R. A. A. and Andrews G. E., "Full Coverage Impingement Heat Transfer at High Temperature," *ASME Paper 90-GT-285,* pp. 1-12, 1990.

[10] Florschuetz, L. W., Truman C. R., and Metzger D. E., "Streamwise Flow and Heat Transfer Distributions for Jet Array Impingement with Cross-flow," *Trans. ASME, J. Heat Transfer,* vol. 103, pp. 337-342, 1981.

[11] Horlock, J. H., Watson D. T., and Jones T. V., "Limitations on Gas Turbine Performance Imposed by Large Turbine Cooling Flows," *J. Eng. for Gas Turbine and Power. Transaction of the ASME,* vol. Vol.123, pp. 487-494, 2001.

[12] Andrews, G.E.; Khalifa, .IM., Planar duct heat transfer with turbulence enhancing obstacles for combustor liner external cooling. In: Proc. ASME IGTI International Gas Turbine Congress: Power for Land, Sea and Air. 2007, Montreal. ASME Paper GT2007–27418, 2007.

[13] Taslim, M.E. and Rosso, N., "Experimental/Numerical Study of Multiple Rows of Confined Jet IMpingement Normal to a Surface at Close Distances". Proc. ASME Turboe Expo 2012, ASME Paper GT2012-68634, 2012.

[14] Lee, C.S., Shih, T.I.P., Bryden, K.M., Ames, R. and Dennis, R.A., "Flow and Heat Transfer in a Jet-Impingment Configuration with no Cross Flows about Impinging Jets". Proc. ASME Turbo Expo 2012, ASME Paper GT2012-70080, 2012.

[15] Andreini, A., Da Soghe, R., Facchini, B., Maiuolo, F., Tarchi, L. and Coutandin, D., "Experimental and Numerical Analysis of Multiple Impingment Jet Arrays for an Active Clearance Control System".Proc. ASME Turbo Expo 2012, ASME Paper GT2012-68791, 2012.

[16] Andrews, G. E. and Hussain C. I., "Full Coverage Impingement Heat Transfer: Influence of Channel Height," presented at the Eight International Heat Transfer Conference, 1986.

[17] Andrews, G. E. and Hussain C. I., "Full Coverage Impingement Heat Transfer: The Influence of Cross-flow," *AIAA-87-2010,* pp. 1-9, 1987.

[18] Andrews, G. E., Abdul Husain R. A. A., and Mkpadi M. C., "Enhanced Impingement Heat Transfer: The Influence of Impingement X/D for Interrupted Rib Obstacles (Rectangular Pin Fins)," *J. Turbomachinery. Trans. ASME,* vol. 128 pp. 321-331, 2006.

[19] Andrews, G. E., Asere A. A., Hussain C. I., and Mkpadi M. C., "Full Coverage Impingement Heat Transfer: The Variation in Pitch to Diameter Ratio at a Constant Gap," *Proportion and Energetics Panel of AGARD, 65th Symposium, 'Heat Transfer and Cooling in Gas Turbines',* ASME Paper 26, pp. 1-12, 1985.

[20] Abdul Husain, R. A. A., Andrews G. E., Asere A. A., and Ndiema C. K. W., "Full Coverage Impingement Heat Transfer: Cooling Effectiveness," *ASME Int. Gas Turbine Conference,* ASME Paper 88-GT-270, pp. 1 - 9, 1988.

[21] Metzger, D.E. and Korstad, R.J., 'Effects of crossflow on impingement heat transfer', ASME J. Eng. Power, p. 73-82, 1970.

[22] Dyban, E. P., Mazur A. I., and Golovanov V. P., "Heat Transfer and Hydrodynamics of an Array of Round Impinging Jets with One-sided Exhaust of the Spent Air," *Int. J. Heat Mass Transfer,* vol. Vol.23, pp. pp.667-676, 1980.

[23] Saad, N. R., Mujumdar A. S., Abdel Messah W., and Douglas W. J. M., "Local Heat Transfer Characteristics for Staggered Arrays of Circular Impinging Jets with Cross-flow of Spent Air," *ASME paper No. 80-HT-23,* pp. 1-8, 1980.

[24] Stoy, R. L. and Ben-haim Y., "Turbulent Jets in a Confined Cross-flow," *Trans. ASME J. Fluid Eng.* pp.551-556, 1973 . ASME Paper 73-FE-15.

[25] Gauntner, J. W., Gladden H. J., Gauntner D. J., and Yeh F. C., "Cross-flow Effects on Impingement Cooling of a Turbine Vane," NASA TM-X3029, 1974.

[26] Obot, N. T. and Trabold T. A., "Impingement Heat Transfer within Arrays of Circular Jets: Part 1-Effects of Minimum, Intermediate and Complete Cross-flow for Small and Large Spacings," *Trans. ASME. J. Heat Transfer,* vol. 109, pp.872-879, 1987.

[27] Bailey, J. C. and Bunker R. S., "Local Heat Transfer and Flow Distributions for Impinging Jet Arrays of Dence and Sparse Extent.," *Paper No. GT-2002-30473,* 2002.

[28] Bailey, J. C., Intile J., Fric T. F., Tolpadi A. K., Nirmalan N. V., and Bunker R. S., "Experimental and Numerical Study of Heat Transfer in a Gas Turbine Combustor Liner," *J. Eng. Gas Turbines and Power. Transactions of the ASME,* vol.125, pp.994-1002, 2003.

[29] Wang, X., Liu R., Bai X., and Yao J., "Numerical Study on Flow and Heat Transfer Characteristics of Jet Impingement," *Proc. ASME Turbo Expo.,* ASME Paper GT2011-45287, pp.1-10, 2011.

[30] Rao, G. A., Levy Y., and Belinkov M. K., "Numerical Analysis of a Multiple Jet Impingement System," in *Proc. ASME Turbo Expo 2009*, ASME Paper GT2009- Florida, 2009, pp. 1-11.

[31] Anand, K. and Jubran B. A., "Computational Study of Micro-jet Impingement Heat Transfer in a High Pressure Turbine Vane," in *Proc. ASME Turbo Expo 2011*, ASME Paper GT2011-45267, pp. 1-12.

[32] Sharif, M. A. R. and Mothe K. K., "Parametric Study of Turbulent Slot-Jet Impingement Heat transfer from Concave Cylindrical Surfaces," *Int. J. Thermal Sciences. Elsevier,* vol. 49, pp. 428-442, 2010.

[33] Kini, C. R., Shenoy B. S., and Sharma N. Y., "A Computational Conjugate Thermal Analysis of HP Stage Turbine Blade Cooling with Innovative Cooling Passage Geometries," in *Proc. Worid Congress on Eng'g*, London, 2011, pp. 1-6.